Atmos. Chem. Phys. Discuss., 15, 30987–31024, 2015
www.atmos-chem-phys-discuss.net/15/30987/2015/
doi:10.5194/acpd-15-30987-2015

Atmospheric Chemistry and Physics Discussions

Long-term trends of surface ozone and its influencing factors at the Mt. Waliguan GAW station, China – Part 1: Overall trends and characteristics

W. Y. Xu[1], W. L. Lin[2], X. B. Xu[1], J. Tang[2], J. Q. Huang[3], H. Wu[3], and X. C. Zhang[2]

[1]Key Laboratory for Atmospheric Chemistry, Institute of Atmospheric Composition, Chinese Academy of Meteorological Sciences, Beijing, China
[2]Meteorological Observation Center, China Meteorological Administration, Beijing, China
[3]Waliguan Observatory, Qinghai Meteorological Bureau, Xining, China

Received: 21 July 2015 – Accepted: 27 October 2015 – Published: 6 November 2015

Correspondence to: X. B. Xu (xuxb@cams.cma.gov.cn)

Published by Copernicus Publications on behalf of the European Geosciences Union.

Abstract

Tropospheric ozone is an important atmospheric oxidant, greenhouse gas and atmospheric pollutant at the same time. The level of tropospheric ozone, particularly in the surface layer, is impacted by emissions of precursors and is subjected to meteorological conditions. Due its importance, the long-term variation trend of baseline ozone is highly needed for environmental and climate change assessment. So far, studies about the long-term trends of ozone at representative sites are mainly available for European and North American sites. Similar studies are lacking for China, a country with rapid economic growth for recent decades, and many other developing countries. To uncover the long-term characteristics and trends of baseline surface ozone, concentration in western China, measurements at a global baseline Global Atmospheric Watch (GAW) station in the north-eastern Tibetan Plateau region (Mt. Waliguan) for the period of 1994 to 2013 were analysed in this study, using a modified Mann–Kendall test and the Hilbert–Huang Transform analysis for the trend and periodicity analysis, respectively. Results reveal higher surface ozone during the night and lower during the day at Waliguan, due to mountain-valley breezes. A seasonal maximum in summer was found, which was probably caused by enhanced stratosphere-to-troposphere exchange events and/or by tropospheric photochemistry. Analysis suggests that there is a season-diurnal cycle in the three-dimensional winds on top of Mt. Waliguan. Season-dependent daytime and nighttime ranges of 6 h were determined based on the season-diurnal cycle in the three-dimensional winds and were used to sort subsets of ozone data for trend analysis. Significant increasing trends in surface ozone were detected for both daytime (1.5–2.7 ppbv $10\,a^{-1}$) and nighttime (1.3–2.9 ppbv $10\,a^{-1}$). Autumn and spring revealed the largest increase rates, while summer and winter showed relatively weaker increases. The HHT spectral analysis confirmed the increasing trends in surface ozone concentration and could further identify four different stages with different increasing rates, with the largest increase occurring around May 2000 and October 2010. A 2–4, 7 and 11 year periodicity was found in the surface ozone concentration. The re-

ACPD
15, 30987–31024, 2015

sults are highly valuable for related climate and environment change assessments of western China and surrounding areas, and for the validation of chemical-climate models.

1 Introduction

Ozone (O_3) is one of the key atmospheric species and is closely related to climate change and environmental issues (IPCC, 2013). The stratospheric ozone layer protects living organisms at the Earth's surface against the harmful solar UV radiation, while tropospheric ozone is an important greenhouse gas and governs oxidation processes in the Earth's atmosphere through formation of OH radical (Staehelin et al., 2001; Lelieveld and Dentener, 2000). In the surface layer, ozone is also one of the toxic gases for human beings and vegetation.

Since stratospheric ozone is much higher in concentration than tropospheric ozone, it can be well monitored by satellites with retrieved column density. However, ozone in the troposphere, particularly surface ozone is highly variable in space and time. Since it is a secondary gas pollutant, surface ozone is not only influenced by local photochemistry, but also by nearby photochemical production of ozone or anthropogenic emissions of ozone precursors, which could reach the measurement site via transport processes (Wang et al., 2006a; Lal et al., 2014). Deep convection and stratosphere-to-troposphere exchange (STE) events can also bring down ozone-rich air from above and influence local surface ozone concentrations (Bonasoni et al., 2000; Ding and Wang, 2006; Stohl et al., 2000; Tang et al., 2011; Lefohn et al., 2012; Jia et al., 2015; Ma et al., 2014; Langford et al., 2009, 2015; Lin et al., 2012a, 2015a). All these influencing factors make it very hard to obtain the background ozone concentration and to understand the causes of observed ozone trends.

Many Global Atmosphere Watch (GAW) stations of the World Meteorological Organization (WMO) and environmental monitoring sites have been setup to monitor surface ozone due to its importance and due to the urgent need to evaluate the trends of back-

ACPD
15, 30987–31024, 2015

ground ozone. Past trends in surface background ozone have been reported for Europe and North America (Cooper et al., 2010; Cui et al., 2011; Gilge et al., 2010; Oltmans et al., 2013; Vingarzan, 2004), which mostly revealed strong increases in ozone before 2000 and slow or even no growth afterwards. Data from some important regions, e.g., East Asia and South America, are very scarce. China, as one of the rapidly developing countries, is contributing increasing ozone precursor concentrations to the atmosphere and was thought to be most responsible for the increase in ozone in the western United States (Cooper et al., 2010), though other studies would suggest that STE events had an equivalent important role in causing high ozone concentrations at the US west coast (e.g., Ambrose et al., 2011). A most recent studies by Lin et al. (2015b) reported insignificant increasing trends for western US during 1995–2014 and by revisiting the work of Cooper et al. (2010) they found overestimated trends during 1995–2008 due to sampling biases. Nevertheless, the impact of Asian outflow on western US ozone concentrations is highly evident (Lin et al., 2012b; Lin, 2015).

Long-term trends in ozone in China, however, were seldom reported. Ding et al. (2008) studied the tropospheric ozone climatology over Beijing based on aircraft data and found a 2 % increase of boundary layer ozone from the period of 1995–1999 to 2000–2005 in Beijing in the North China Plain (NCP) region, which was mostly driven by the increasing anthropogenic emissions in the surrounding regions. Upper tropospheric ozone displayed weaker increasing trends. Wang et al. (2012) reported a similar increasing trend of lower tropospheric ozone and a larger upper tropospheric ozone increase for the period of 2002 to 2010 based on ozonesonde measurements in Beijing. Xu et al. (2008) observed positive trends and increased variability in ozone at Lin'an, a background site in the Yangtze River Delta (YRD) region. Wang et al. (2009) found a significant increasing trend of 0.58 ppbv yr^{-1} during 1994 to 2007 at a coastal site of Hong Kong in the Pearl River Delta (PRD) region, which were caused by rapid increases in ozone precursor emissions in the upwind source regions. The above studies were all carried out in the eastern part of China, in the three most polluted regions NCP, YRD and PRD. Observed ozone concentrations were mainly under the influence

ACPD
15, 30987–31024, 2015

of regional air pollution and are not representative of the background ozone level on a larger scale. The trends of ozone over other parts of China remain to be studied based on long-term observations.

Continuous long-term observations of surface ozone are made only at a few representative sites, among which is the Mt. Waliguan (WLG) GAW station. The WLG station, established in 1994, is situated in the northeastern edge of the Tibetan Plateau, where population is scarce and industries hardly exist. A few studies have already been performed on short-term measurements of ozone at WLG. Past research already revealed that surface ozone at the site is highly representative of free-tropospheric ozone (Ma et al., 2002b) and is often influenced by stratosphere-to-troposphere exchange (STE) events (Ding and Wang, 2006; Zhu et al., 2004). Air masses from the west are dominant at WLG and were associated with the highest ozone concentrations (Wang et al., 2006b). Only in summer a substantial part of the airflows come from the eastern sector and exposes the surface ozone concentration to some regional anthropogenic influences (Wang et al., 2006b; Xue et al., 2011). Other than STE, meteorological factors with very short timescales such as the diurnal cycle in topographic wind or with very long timescales such as the solar cycle also have significant impacts on tropospheric ozone at WLG (Huang et al., 2009; Wang et al., 2006b; Zhang et al., 2009). QBO (Quasi Bi-annual Oscillation) and ENSO (El Niño and Southern Oscillation) have been proved to be significant influencing factors on the total ozone at WLG (Ji et al., 2001; Zou et al., 2001), which could potentially affect tropospheric ozone as well. Voulgarakis et al. (2011) suggest that the change in dynamics after El Niño events hardly leads to changes in stratospheric ozone, but can promote the cross-tropopause ozone exchange and lead to the rise in global tropospheric ozone concentration. Lin et al. (2015a) found that El Niño events only enhanced upper tropospheric ozone, which could not reach the surface. Springs following strong La Niña winters, however, displayed increasing frequencies in stratospheric intrusions and increased surface ozone concentrations. Their model results show that this is the mechanism that contributes

ACPD
15, 30987–31024, 2015

the most to the inter-annual variability of ozone in the western US during spring, while Asian pollution and wildfires had very little impact.

Past studies of ozone at WLG were all based on short-term measurements and were most mechanism studies, which often reached controversial results and brought upon debates (Ma et al., 2002a, 2005; Zhu et al., 2004), while the overall variation characteristics and long-term trend of ozone at WLG remain unclear. In this study, we present an analysis of 20 year surface ozone concentration at WLG. Besides unravelling the characteristics of ozone variations and the overall variation trend of ozone, a precise and adaptive spectral analysis method will be applied to investigate the trend during different periods and the underlying periodicities within the data.

2 Data and methodology

2.1 Site and measurements

The Mt. Waliguan site (WLG, 36°17′ N, 100°54′ E, 3816 m a.s.l.) is located in Qinghai Province, China. It is one of the global baseline stations of the WMO/GAW network and the only one in the hinterland of Eurasia continent. Mt. Waliguan is situated at the northeast edge of the Qinghai-Tibetan Plateau and surrounded by highland steppes, tundra, desserts, salt lakes, etc. (Fig. 1). With very few population (about 6 persons km^{-2}) and nearly no industry within 30 km, the WLG site is far from major anthropogenic sources. However, some impact of long-range transport of anthropogenic pollutants from the NE-SE sector cannot be excluded, particularly from the major cities Xining (about 90 km northeast of WLG, population ∼ 2.13 millions) and Lanzhou (about 260 km east of WLG, population ∼ 3.1 millions). Such impact, if any, may be significant only during the warmer period (May–September), as suggested by past airmass trajectory studies (Zhang et al., 2011).

The WLG baseline station was established in 1994. Long-term monitoring program for surface ozone began in August 1994. The concentration of surface ozone has been

ACPD
15, 30987–31024, 2015

measured using two ozone analysers (Model 49, Thermal Environmental Instruments; one of the analyzers was replaced with a Model 49i ozone analyzer in 2011). The analysers have been automatically zeroed alternatively every second day by introducing ozone-free air for 45 min. Seasonal multipoint calibrations have been done using an ozone calibrator (Model 49PS, Thermal Environmental Instruments). In the years 1994, 1995, 2000, 2004, and 2009, the ozone calibrator and analysers at WLG were compared with the transfer standard from the WMO World Calibration Centre for Surface Ozone and Carbon Monoxide, EMPA Dübendorf, Switzerland. Intercomparison results show excellent or good agreement between the WLG instruments and the transfer standard (Zellweger et al., 2000, 2004, 2009). Surface ozone data are recorded every 5 min and corrected annually based on the zero-checks and multipoint calibrations. If the observed ozone values from the two analysers agree within 5 ppb, average values are calculated and included in the final dataset. Otherwise, causes for the differences are searched by the principal investigator and only data from the well-performing analyser are included in the dataset. Ozone concentrations in 5 min resolution from August 1994 to December 2013 were averaged into hourly data and used in this study. In the trend analysis, monthly average ozone concentrations were acquired by first calculating the daily average ozone, values and then performing a monthly averaging. A data completeness of 75 % was required for each averaging step.

Meteorological observations have been made at the site using automatic weather stations (AWS) installed on the ground level and on an 80 m tower at 2, 10, 20, 40 and 80 m. These observations provide meteorological parameters such as temperature, pressure, precipitation, and wind speed/direction in 5 min resolution. Additionally, the vertical velocity is measured at the 80 m platform. The 10 m horizontal wind and 80 m vertical wind data from August 1994 to December 2013 are used in this study and have been accordingly averaged into hourly data, which meet a data completeness requirement of 75 %.

ACPD
15, 30987–31024, 2015

2.2 Determination of daytime and nighttime

Past research has already revealed that the surface ozone at WLG is governed by different air masses during daytime and nighttime (Ma et al., 2002b). The WLG station experiences upslope winds during the day and is controlled by boundary layer (BL) air, while during the night, winds go downslope and the site is controlled by free tropospheric (FT) air. The boundary layer air is largely influenced by local photochemistry and contains pollutants transported from nearby areas, while the free-tropospheric air represents the background ozone and may sometimes contain signals of long-range transport or STE events. Hence, it is of necessity to differentiate daytime and nighttime ozone concentration in order to study the trend signals brought by different air masses.

In the previous study (Xu et al., 2011), daytime and the nighttime were defined as a fixed time ranges (e.g. 11:00–16:00 LT for daytime and 23:00–4:00 LT for nighttime). However, the actual well-developed day and night time range varies with season. So does the local wind. Figure 2a–c respectively shows the season-diurnal variation characteristics of 10 m zonal ($\boldsymbol{u}$) and meridional ($\boldsymbol{v}$) wind velocity and the 80 m vertical (ω) wind velocity. Due to the local topography, the WLG station is under the influence of mountain-valley breezes and all three wind vectors exhibit distinct diurnal variation characteristics. The height difference to the west of Mt. WLG is much larger than that to the east, hence valley breezes during daytime come from the west accompanied by upward drafts, resulting in a diurnal maximum $\boldsymbol{u}$ and $\boldsymbol{w}$ vector between noontime and middle afternoon depending on season. The $\boldsymbol{v}$ vector changes from southern winds to northern winds around noontime. Mountain breezes during the night come from the east-south sector accompanied by subsiding air flows, resulting in low $\boldsymbol{u}$ and $\boldsymbol{w}$ and high $\boldsymbol{v}$ during the night. The dominant air flow at WLG is westerly during the cold seasons, which enhances the westerly valley breeze during the day and cancels out the easterly mountain breeze during the night. During the warm seasons, easterly winds gain in frequency, which sometimes cancels out the daytime valley breeze and enhances the nighttime mountain breeze. The distinct diurnal variation of the wind can be

ACPD
15, 30987–31024, 2015

used to define a daytime and nighttime range that varies with season. The white dots in Fig. 2 represent the monthly average occurrence hour of the diurnal maximum $\boldsymbol{u}$. In this study, a 6 h time range that is centred around the white dots is used as the daytime range (white dashed lines in Fig. 2). The nighttime range also covers 6 h and leaves a 6 h transition stage after the end and before the start of the daytime range.

2.3 Trend analysis

The trend analysis was performed using a both spearman's linear trend analysis and the modified Mann–Kendall's trend test. Here, a brief description on the modified Mann–Kendall test will be given. The Mann–Kendall test is a non-parametric test commonly used to detect trends. Hamed and Ramachandra Rao (1998) modified the test, so that it can be used on data with seasonality.

For two sets of observations $X = x_1, x_2, \ldots, x_n$ and $Y = y_1, y_2, \ldots, y_n$, the rank correlation test as proposed by Kendall (1955) is performed as the following:

$$S = \sum_{i<j} a_{ij} b_{ij} \tag{1}$$

Where

$$a_{ij} = \operatorname{sign}\left(x_j - x_i\right) = \begin{cases} 1 & x_i < x_j \\ 0 & x_i = x_j \\ -1 & x_i > x_j \end{cases} \quad \text{and } b_{ij} \text{ is the equivalent for } Y. \tag{2}$$

If Y is replaced with the time order $T = 1, 2, \ldots, n$, the test becomes a trend test and $S = \sum_{i<j} a_{ij}$. The significance of the trend is tested by comparing the standardized test statistic $Z = S/\sqrt{\operatorname{var}(S)}$ to the standard normal variate at a given significance level (Z_α). Here, a modified var(S) is given by:

$$\operatorname{var}(S) = \frac{n(n-1)(2n+5)}{18} \frac{n}{n_S^*}, \tag{3}$$

ACPD
15, 30987–31024, 2015

where $\frac{n}{n_S^*}$ represents a correction for the autocorrelation that exists in the data and can be obtained by an approximation to the theoretical values.

$$\frac{n}{n_S^*} = 1 + \frac{2}{n(n-1)(n-2)} \sum_{i=1}^{n} (n-i)(n-i-1)(n-i-2)\rho_s(i) \quad (4)$$

Here $\rho_s(i)$ is the autocorrelation function of the ranks of the observations.

If $|Z| > Z_{1-\alpha/2}$, then the data is non-stationary, a positive Z would indicate a positive trend and a negative Z would suggest a declining trend. If $|Z| > Z_{1-\alpha/2}$, then the data is stationary. Here we use $\alpha = 0.05$, hence the corresponding critical $Z_{1-\alpha/2} = 1.96$. A non-parametric method is then used to estimate the slope of the trend, details can be found in Sen (1968).

2.4 The Hilbert–Huang transform analysis

The Hilbert–Huang Transform (HHT) analysis is a combination of the Empirical Mode Decomposition (EMD) and the Hilbert Spectral analysis proposed by (Huang et al., 1998). It is often used to analyse the time-frequency variation of non-linear and non-stationary processes. The EMD acts as a time-frequency filter, it decomposes the data into several oscillation modes with different characteristic time scales. The HHT method has proved to be an efficient and precise method in investigating the periodicity, long-term oscillations and trends that are embedded within the data (Huang and Wu, 2008). So far, it has been widely applied in atmospheric and climatic studies including wind field, temperature and rainfall analysis (Rao and Hsu, 2008; Lundquist, 2003; El-Askary et al., 2004), but it has not been used on atmospheric composition data yet. Here we give a brief description of the HHT method.

First, the EMD is performed on the data, to decompose the data into n intrinsic mode functions (IMF), $c_1, c_2 \ldots, c_n$, and one residual r_n, which are ordered from the smallest

ACPD
15, 30987–31024, 2015

to the largest variational time scale (Huang et al., 2003).

$$x(t) = \sum_{j=1}^{n} c_j + r_n \tag{5}$$

Then the Hilbert transform is applied to each IMF using Eq. (6),

$$y(t) = \frac{1}{\pi} P \int_{-\infty}^{\infty} \frac{x(t')}{t - t'} \mathrm{d}t' \tag{6}$$

Where P is the Cauchy principal value. An analytical signal is then obtained with Eq. (7),

$$z(t) = x(t) + iy(t) = a(t)\, e^{i\theta(t)}, \tag{7}$$

where,

$$a(t) = [x^2(t) + y^2(t)]^{1/2} \text{ and } \theta(t) = \arctan\left(\frac{y(t)}{x(t)}\right). \tag{8}$$

The instantaneous frequency ω can be calculated as the following:

$$\omega(t) = \frac{\mathrm{d}\theta(t)}{\mathrm{d}t}. \tag{9}$$

Thus, Eq. (5) an be transformed into the following expression:

$$x(t) = \mathcal{R} \sum_{j=1}^{n} a_j(t) \exp\left(i \int \omega_j(\tau)\, \mathrm{d}\tau\right), \tag{10}$$

where $\mathcal{R}$ is the real part of the complex number.

ACPD
15, 30987–31024, 2015

To obtain the Hilbert amplitude sprectrum $H(\omega,t)$, we assign for each time t, the calculated amplitude $a_j(t)$ to the according $\omega_j(t)$. An integration of $H(\omega,t)$ over the frequency span would yield the instantaneous energy (IE), which represents the time variation of the energy. An integration along the time span would yield the marginal Hilbert spectrum $h(\omega)$, which provides information on how the frequency is distributed over the entire span.

The degree of stationarity DS(ω) is often used to investigate the stationarity and periodicity of the data, it is defined as:

$$\mathrm{DS}(\omega) = \frac{1}{T}\int_0^T \left(1 - \frac{H(\omega,t)}{h(\omega)/T}\right)^2 \mathrm{d}t, \tag{11}$$

where T is the entire time span.

The volatility which is defined as the ratio of the sum of certain IMF components $S_h(t)$ to the original signal $S(t)$, here we use the summation of residual and all the IMFs but the first one as $S_h(t)$:

$$V(t,T) = \frac{S_h(t)}{S(t)} = \frac{\sum_{j=2}^{n} c_j(t) + r(t)}{S(t)}, \tag{12}$$

where n is the number of IMFs.

2.5 The gap-filling of the monthly average ozone data

To perform the HHT analysis, a complete, even-spaced dataset is required. Hence we need to fill the gaps in the monthly average surface ozone, concentration data. The location of the gaps can be seen in Fig. 4b. It can be noted that gaps could be found in 1997, 1998, 1999 and 2002. If the gap is small and occurs in between the ozone seasonal low and peak value, then a spline interpolation would suffice. However, this

ACPD
15, 30987–31024, 2015

is not the case for some gaps. In 1997 and 1998, the gaps occur during summertime, when ozone concentration should be highest. In 2002, the gap continues on to winter, when ozone concentration should be lowest. A simple spline interpolation would underestimate the seasonal peak value and overestimate the seasonal low. Hence, we applied the following method to fill the gaps.

First, the monthly mean ozone timeseries during 1994 to 2013, as is shown in Fig. 4b, is shaped into an array $O_3(i,j)$ of the size [20 years × 12 months], where $i = 1994, \ldots,$ 2013 and $j = 1, \ldots, 12$.

The gaps in $O_3(i,j)$ are filled by applying a spline interpolation on each row of the array:

$$O_{3,\text{spline}}(1994,\ldots,2013,j) = \text{spline}(O_3(1994,\ldots,2013,j)) \quad j = 1,\ldots,12 \tag{13}$$

In this way, both the average value of ozone concentration, at a certain month and the overall ozone variation trend will be considered. A complete dataset of average monthly ozone concentration can then be recreated by using interpolated data only on months of missing observation data:

$$O_{3,\text{complete}} = \begin{cases} O_{3,\text{spline}}, & \text{missing } O_3 \\ O_3, & \text{existing } O_3 \end{cases} \tag{14}$$

The result is displayed in Fig. 7a, with the original data in solid lines and interpolated data in dashed lines. Our method could yield a reasonable interpolated timeseries with both seasonal low and peak values occurring at the right time of year.

3 Results and discussion

3.1 Season-diurnal variation characteristics of ozone

The average season-diurnal variation of surface ozone during 1994 to 2013 is displayed in Fig. 3. The seasonal maximum ozone occurs during summer, with an average peak

ACPD
15, 30987–31024, 2015

in June–July, while the minimum is found in winter (Fig. 3a), which will be discussed in detail in Sect. 3.2.

Daily maximum ozone usually occurs during nighttime, while the daily minimum ozone is found around noontime, on average at 12 a.m., Beijing Local Time (Fig. 3c). Ma et al. (2002b) suggest that the WLG station is mostly influenced by boundary layer (BL) air that is brought up through an upslope flow during the day, while a downslope flow brings down free tropospheric (FT) air during the night. The BL air masses are typically characterised by lower ozone concentrations in comparison with FT air masses, hence the occurrence of the daily ozone minimum value indicates the time when the BL is fully developed and the air within is well mixed.

From Fig. 3b it can be denoted that, the occurrence time of the daily minimum ozone concentration (white dots) shows a significant seasonal variation similar to that of the zonal and vertical wind velocity (Fig. 2). Due to the seasonal variation of the development of the boundary layer, the daily minimum ozone, should occur earlier in the day during warm seasons and later in the day during cold seasons. This phenomenon can indeed be confirmed by Fig. 3b, however, the ozone minimum of June–August seems to occur later than expected. This phenomenon could not been found in the season-diurnal variation of horizontal or vertical wind speeds, thus it is not caused by boundary layer development. A possible explanation might be that the photochemical production of ozone was enhanced at early noon during summertime, leading to a delayed noontime minimum. The in-situ ozone production/destruction in different seasons is not well quantified at the moment. Past researches focused on modelling the photochemical net production in spring and summer and reached to controversial conclusions (Ma et al., 2002b; Wang et al., 2015). Hence there is a need for more investigation into the cause for such a phenomenon.

3.2 Season-annual variation characteristics of ozone

Figure 4 displays the season-annual variation of surface ozone during 1994 to 2013. Again, the ozone concentration peaks in summer and is lowest during winter (Fig. 4b),

ACPD
15, 30987–31024, 2015

with an average seasonal peak occurring in June during 1994 to 2013 (Fig. 4c). Previous studies reported the same seasonal ozone pattern, but attributed the summertime peak to different causes, e.g., more frequent STE events (Ding and Wang, 2006; Tang et al., 2011), enhanced vertical convection (Ma et al., 2005), long-range transport from eastern-central China, central-southern Asia or even Europe during summer (Zhu et al., 2004) and stronger cross boundary transport and vertical convection during the East Asian summer monsoon season (Yang et al., 2014). From Fig. 2c it can be noted that nighttime subsiding wind is indeed strongest in summer, which supports the hypothesis of downward transport of ozone. Zheng et al. (2011) argue that STE reaches maximum strength in spring and shows a decline in late spring based on $^{10}Be/^{7}Be$ measurements, indicating that the continuous ozone increase in summer is caused by the photochemical production.

The long-term variation of the annual average ozone exhibits a clear increasing trend (Fig. 4a). A 2–4 year cycle seems to exist within the long-term variation of surface ozone. Past research has shown that there is a quasi-biannual oscillation (QBO) within the ozone column density over the Tibetan Plateau, which is in antiphase with the QBO of the tropical stratospheric winds, exhibiting a 29 month cycle (Ji et al., 2001). The WLG station, with its high altitude, is very representative of the tropospheric background and also highly influenced by STE. Thus, the surface ozone at WLG might also have a QBO that is related to that of the total ozone, column.

3.3 Long-term variation trends of ozone

The trends of monthly average all-day, daytime and nighttime ozone during 1994 to 2013 are displayed in Fig. 5a1–c1, respectively. Ozone data in Fig. 5b1 and c1 are the subsets of data from the daytime and nighttime ranges determined in Sect. 2.2. The increase in surface ozone in the past two decades is evident in all three data subsets, with a slightly stronger increase in the nighttime data. The linear trends for all-day, daytime and nighttime ozone concentrations reached 2.5, 2.4 and 2.8 ppbv 10 a^{-1}, respectively, while the Kendall slopes reached 1.8, 1.7, 1.9 ppbv 10 a^{-1}, respectively.

ACPD
15, 30987–31024, 2015

The Kendall slope is smaller than the linear regression slope, mainly because the linear regression method does not consider the seasonality within the data. However, both methods yielded statistically significant increasing trends.

To further investigate the trend in ozone in different seasons, the trend of seasonal average ozone, during 1994 to 2013 was calculated and are shown in Fig. 5a–c (2–5). After eliminating the seasonality in the data, the linear least squares fitting slopes and Kendall's slope yielded very similar results, thus we only listed the linear slopes and p values in Table 1. The strongest increase in surface ozone was found in autumn (SON), followed by spring (MAM), respectively reaching 2.8 and 2.4 ppbv $10\,a^{-1}$ in the seasonal average of all-day ozone concentrations. In comparison, summer (JJA) and winter (DJF) both showed much weaker increasing trends, with rates of 1.5 and 1.4 ppbv $10\,a^{-1}$, respectively, amongst which the summertime trend could not even reach a confidence level of 95 %. In summer the daytime increasing rate is significantly lower than the nighttime one, respectively reaching 0.7 and 2.2 ppbv $10\,a^{-1}$. The nighttime slope reached the confidence level of 95 %, while the daytime slope is statistically insignificant.

Past investigations on the air-mass origin of WLG have shown that WLG is mostly governed by western and northwestern air-masses, air-masses coming from the eastern sector takes up only 2, 5 and 8 % in winter, spring and autumn, respectively (Zhang et al., 2011). However, in summer there is a significant percentage (30 %) of air-masses coming from the eastern direction. Since the two major cities in the vicinity of WLG are both in the east, summertime is believed to be the season in which WLG is most influenced by nearby anthropogenic activities. From the diurnal variation of the horizontal wind speeds (Fig. 2a–b) it can be discerned that daytime winds are weak northern winds, while nighttime winds are rather strong north-easterly winds, which are more in favour of transporting anthropogenic pollution to WLG.

As already mentioned before in Sect. 3.2, some research believe that STE is also most frequent in summer at WLG (Ding and Wang, 2006). During the night the WLG site is governed by downwards winds, which may bring down air with high ozone con-

ACPD
15, 30987–31024, 2015

centrations from above. Hence, an increase in the frequency of STE events would also result in increasing nighttime ozone concentrations in summer. Whether it is anthropogenic activities or rather meteorological factors, that has led to significantly distinct daytime and nighttime ozone variation slopes, still needs further investigations and will be discussed in Part 2 of our study (Xu et al., 2015).

The seasonal ozone peak in the Northern Hemisphere typically occurs in spring, which is believed to be the result of enhanced photochemical production in spring (Monks, 2000; Vingarzan, 2004). The seasonal ozone peak at WLG occurs in summer, however, the largest increase in ozone concentration was found in autumn rather than spring or summer. Lin et al. (2014) also reported significant increasing ozone trends in autumn rather than spring at the Mauna Loa Observatory in Hawaii in the past 4 decades and attributed this phenomenon to strengthened ozone-rich air flows from Eurasia. The reason why we observed the largest increase in ozone levels during autumn also needs further exploration and will be handled in Part 2 (Xu et al., 2015).

Here we present a comparison between the seasonal ozone variation trends of all the high altitude (> 1200 m a.s.l.) sites in the Northern Hemisphere (Table 2). The stations have been sorted by latitude. The low latitude sites, Mauna Loa and Izaña, both show increasing trends (3.1 ± 0.7 and 1.4 ± 0.5 ppbv $10\,a^{-1}$) during 1991 to 2010 (Oltmans et al., 2013). Lin et al. (2014) suggested that, in the period of 1995 to 2011 in comparison with the period of 1980 to 1995, the Mauna Loa site in Hawaii displays strong increasing ozone concentrations during summer and autumn. The mid-latitude stations exhibit inconsistent trends. Significantly positive trends were detected in the Rocky Mountains, USA (3.3 ± 0.5 ppbv $10\,a^{-1}$, Oltmans et al., 2013) and at Jungfraujoch, Switzerland (3.2 ± 1.8 ppbv $10\,a^{-1}$, Cui et al., 2011). Tarasova et al. (2009) found evidence for increased stratospheric contribution to surface ozone at Jungfraujoch. The strongest increase at Jungfraujoch was detected in winter, the weakest in summer. Gilge et al. (2010) also reported increased wintertime ozone at other two alpine sites in central Europe during 1995–2007. Lin et al. (2015b) reported that springtime free-tropospheric ozone displays an insignificant increasing trend over western North

ACPD
15, 30987–31024, 2015

America during 1995–2014, however, by shutting of North American emissions in the model, the subset of ozone associated with Asian influence and also possibly mixed with stratospheric intrusions revealed a significant increasing rate during 1992–2012. No significant trends were found at Pinadale, USA and Zugspitze, Germany. Negative trends were revealed at Kislovodsk, Russia (-3.7 ± 1.4 ppbv $10\,a^{-1}$, Tarasova et al., 2009) and Whiteface, USA (-2.2 ± 0.6 ppbv $10\,a^{-1}$, Oltmans, 2013). Tarasova et al. (2009) attributed the strong decrease in ozone in Kislovodsk to control measures of Europe and the breakdown of the former USSR. From past literature we can discern that, both the strong increasing and decreasing trends were mostly caused by the variation in ozone concentrations in the 1990 s. The positive trend at Jungfraujoch during the 1990 s was strongest in spring and weakest in summer and autumn, while the reduction at Kislovodsk was strongest in summer and weaker in autumn and winter (Tarasova et al., 2009). After 2000, ozone concentrations have entered a steady stage with either slow or no growth (Tarasova et al., 2009; Oltmans et al., 2013).

In comparison with other sites, Mt. Waliguan shows a continuous rise of ozone concentration throughout the past 2 decades and the most significant positive trends appear in autumn and spring, unlike the other mid-latitude stations. The cause of this phenomenon still needs further exploration.

3.4 Hilbert–Huang spectral analysis of surface ozone, at WLG

The long-term variation of surface ozone may be the result from changes in emissions of ozone precursors, but may also be caused by year-to-year fluctuations or multi-year oscillations of climate conditions. All the related factors have different periodicities, which is why the variation of ozone is highly non-linear. To unravel the potential oscillations on different time scales in the ozone timeseries, we performed an HHT analysis on the ozone data from WLG using the method given in Sect. 2.4. The result of the EMD is shown in Fig. 6. The monthly average ozone signal could be decomposed into 5 IMFs with different characteristic time scales. The lowest order IMF (c1) shows an oscillation with the highest frequency. The second IMF (c2) shows the seasonal varia-

ACPD
15, 30987–31024, 2015

tion in the ozone signal. C3 reveals 3–4 year oscillations, c4 shows 7 year oscillations and the highest order IMF (c5 in Fig. 6f) shows the longest oscillations pattern, with a quasi-10 year periodicity.

Segmentations is performed by finding the local extrema of c5. The total time span could be separated into 4 segments, as indicated by the dotted lines in Fig. 6a. The slope of the segments of c5 can indicate whether the value is increasing or declining. To determine the significance of the trend, the modified Mann–Kendall trend test is performed on each segment and the results are given in Table 3. The first segment lasts 3 years (from August 1994 to June 1997) and reveals no significant trend (z = 1.42), with an increasing slope of 2.7 ppbv 10 a^{-1}. The second segment lasts for 5 years (from July 1997 to May 2002) and displays a significant upward trend (z = 3.66). The increasing slope reaches 4.2 ppbv 10 a^{-1}. Afterwards the increasing speed of ozone concentrations at WLG slows down in segment 3, lasting 6 years (from June 2002 to April 2008), with a variation slope of 3.0 ppbv 10 a^{-1}, however, the increasing trend remains significant (z = 3.57). In the last segment, which starts in May 2008 and ends in July 2013, the significant upward trend continues (z = 3.65) with a larger increasing slope (3.6 ppbv 10 a^{-1}) than that in segment 3.

Overall, surface ozone concentration at WLG has been rising continuously since 1997. Figure 7a shows the anomaly of the interpolated monthly average ozone during 1994 to 2013, its overall variation trend (represented by c5 + r in Fig. 6) and its variation on a scale of 7 year or longer (represented by c4 + c5 + r in Fig. 6). The corresponding variation slopes of the overall variation trend and the 7 year or longer variation is depicted in Fig. 7b. The overall variation trend confirms the continuous increase since January 1997. The two largest slopes are respectively detected in May 2000 and October 2010. The 7 year or longer trend line displays a rise in ozone after August 1996, which reaches a maximum increasing speed in September 2003. Afterwards, the increase slows down and turns into a decreasing trend in September 2005. After January 2009, ozone concentrations went up again, reaching a maximum increasing speed in December 2010.

ACPD
15, 30987–31024, 2015

The Hilbert Energy Spectrum is depicted in Fig. 8d, along with the volatility, instantaneous energy (IE) and the degree of stationarity (DS) (Fig. 8b, c, e). Both the volatility and the IE reflect the variation of energy with time. Compared to the mean IE, which represents the temporal variation of the frequency averaged energy, volatility rather focuses on the ratio of the variation of certain signals to the total signal. Peaks in the mean IE could be found in 1994–1995, 2000–2001, 2003, 2008 and 2013, which corresponds to the high ozone, concentration values in the data. High values of volatility were found around 2003, 2008 and 2012, which mostly agree with those of the IE. The cause for these high anomalies still needs to be investigated upon.

The Ds corresponding to each frequency, as displayed in Fig. 8e, can provide information on the underlying periodicity within the original signal. The smaller Ds is, the more stationary the data is at this frequency. The lower Ds values are observed in the low frequency part. A dip-down at the frequencies between 0.08 and 0.12 could be found, which corresponds to the annual cycle of ozone. Other dip-downs are found at even lower frequencies, corresponding to 2.5a, 3.5a, 7a and 11a cycles. Among all the known atmospheric factors that have an impact on the ozone concentration at WLG, QBO has a quasi-2 year cycle, ENSO bears a 2 to 7 year cycle and solar activities vary with a 11 year cycle. The combined effect of QBO and ENSO could be responsible for the 2.5a or 3.5a periodicity as suggested by the Ds. Further investigations of these periodicities will be carried out in Part 2 (Xu et al., 2015).

4 Summary

In this paper we present the characteristics, trends and periodicity of surface ozone, concentration at a global baseline GAW station in the eastern Tibetan Plateau region (Mt. Waliguan) during the past two decades. The trends and periodicity of ozone were, investigated using a modified Mann–Kendall test and an adaptive method (Hilbert–Huang Transform) that is suited for analysing non-stationary and non-linear natural processes.

ACPD
15, 30987–31024, 2015

Results reveal that surface ozone at Waliguan is higher during the night and lower during the day, because the station is under the control of ozone-rich free-tropospheric air during the night and boundary layer air during the day due to mountain-valley breeze. Ozone displays a seasonal maximum in summer and minimum in winter, which is probably caused by enhanced stratosphere-to-troposphere exchange events and/or by tropospheric photochemistry. Analysis suggests that there is a season-diurnal cycle in the three-dimensional winds on top of Mt. Waliguan. This allows for defining well-development daytime and nighttime ranges that change from month to month. Trends of surface ozone were calculated for the data subsets of the defined daytime and nighttime as well as for all-day in different seasons. Both daytime and nighttime surface ozone has been significantly increasing at Waliguan. Autumn and spring revealed the largest increase rates, while summer and winter showed relatively weaker increases. A significant daytime and nightime difference in trend could only be found in summer, where nighttime ozone was significantly increasing and daytime ozone bears no significant trend. Summer is the season during which Waliguan is mostly influenced by airmasses from the eastern sector. Whether anthropogenic activities in the two nearest major cities in the eastern sector have impacts on the trend of summertime ozone still needs further exploration.

Results of the HHT spectral analysis confirm the increasing trends in surface ozone concentration and could further identify four different stages with different increasing rates. The overall trend indicates that the largest increase occurred around May 2000 and October 2010. The ozone signal was also decomposed into five intrinsic mode functions with different time scales. A 2–4, 7 and 11 year periodicity was found within the data, the cause of which still needs further investigation. The results obtained in this work are very valuable for related climate and environment change assessments of western China and surrounding areas, and for the validation of chemical-climate models.

Acknowledgement. We thank all operators of the Mt. Waliguan Baseline Station for their excellent routine work. We appreciate WMO/GEF, WMO/GAW, Canada/AES, and Swiss/WCC-

ACPD
15, 30987–31024, 2015

Empa for funding and technical support. This work is supported by China Special Fund for Meteorological Research in the Public Interest (No. GYHY201106023), China Special Fund for Environmental Research in the Public Interest (No. 201509002) and the Basic Research Fund of CAMS (No. 2013Z005).

References

Ambrose, J. L., Reidmiller, D. R., and Jaffe, D. A.: Causes of high O3 in the lower free troposphere over the Pacific Northwest as observed at the Mt. Bachelor Observatory, Atmos. Environ., 45, 5302–5315, doi:10.1016/j.atmosenv.2011.06.056, 2011.

Bonasoni, P., Evangelisti, F., Bonafe, U., Ravegnani, F., Calzolari, F., Stohl, A., Tositti, L., Tubertini, O., and Colombo, T.: Stratospheric ozone intrusion episodes recorded at Mt. Cimone during the VOTALP project: case studies, Atmos. Environ., 34, 1355–1365, doi:10.1016/S1352-2310(99)00280-0, 2000.

Cooper, O. R., Parrish, D. D., Stohl, A., Trainer, M., Nedelec, P., Thouret, V., Cammas, J. P., Oltmans, S. J., Johnson, B. J., Tarasick, D., Leblanc, T., McDermid, I. S., Jaffe, D., Gao, R., Stith, J., Ryerson, T., Aikin, K., Campos, T., Weinheimer, A., and Avery, M. A.: Increasing springtime ozone mixing ratios in the free troposphere over western North America, Nature, 463, 344–348, doi:10.1038/nature08708, 2010.

Cui, J., Pandey Deolal, S., Sprenger, M., Henne, S., Staehelin, J., Steinbacher, M., and Nédélec, P.: Free tropospheric ozone changes over Europe as observed at Jungfraujoch (1990–2008): an analysis based on backward trajectories, J. Geophys. Res.-Atmos., 116, D10304, doi:10.1029/2010JD015154, 2011.

Ding, A. and Wang, T.: Influence of stratosphere-to-troposphere exchange on the seasonal cycle of surface ozone at Mount Waliguan in western China, Geophys. Res. Lett., 33, L03803, doi:10.1029/2005GL024760, 2006.

Ding, A. J., Wang, T., Thouret, V., Cammas, J.-P., and Nédélec, P.: Tropospheric ozone climatology over Beijing: analysis of aircraft data from the MOZAIC program, Atmos. Chem. Phys., 8, 1–13, doi:10.5194/acp-8-1-2008, 2008.

El-Askary, H., Sarkar, S., Chiu, L., Kafatos, M., and El-Ghazawi, T.: Rain gauge derived precipitation variability over Virginia and its relation with the El Nino southern oscillation, Adv. Space Res., 33, 338–342, doi:10.1016/S0273-1177(03)00478-2, 2004.

ACPD
15, 30987–31024, 2015

Gilge, S., Plass-Duelmer, C., Fricke, W., Kaiser, A., Ries, L., Buchmann, B., and Steinbacher, M.: Ozone, carbon monoxide and nitrogen oxides time series at four alpine GAW mountain stations in central Europe, Atmos. Chem. Phys., 10, 12295–12316, doi:10.5194/acp-10-12295-2010, 2010.

Hamed, K. H. and Ramachandra Rao, A.: A modified Mann–Kendall trend test for autocorrelated data, J. Hydrol., 204, 182–196, doi:10.1016/S0022-1694(97)00125-X, 1998.

Huang, F.-X., Liu, N.-Q., and Zhao, M.-X.: Solar cycle signal of tropospheric ozone over the Tibetan Plateau, Chinese J. Geophys.-Ch., 52, 913–921, doi:10.1002/cjg2.1416, 2009.

Huang, N. E. and Wu, Z.: A review on Hilbert–Huang transform: method and its applications to geophysical studies, Rev. Geophys., 46, RG2006, doi:10.1029/2007RG000228, 2008.

Huang, N. E., Shen, Z., Long, S. R., Wu, M. C., Shih, H. H., Zheng, Q., Yen, N.-C., Tung, C. C., and Liu, H. H.: The empirical mode decomposition and the Hilbert spectrum for nonlinear and non-stationary time series analysis, P. Roy. Soc. Lond. A Mat., 454, 903–995, 1998.

Huang, N. E., Wu, M.-L. C., Long, S. R., Shen, S. S. P., Qu, W., Gloersen, P., and Fan, K. L.: A confidence limit for the empirical mode decomposition and Hilbert spectral analysis, P. Roy. Soc. Lond. A Mat., 459, 2317–2345, 2003.

IPCC: Climate Change 2013: The Physical Science Basis. Contribution of Working Group I to the Fifth Assessment Report of the Intergovernmental Panel on Climate Change, Cambridge Univ. Press, Cambridge, UK and New York, NY, USA, 1535, 2013.

Ji, C. P., Zou, H., and Zhou, L. B.: QBO Signal in Total Ozone Over the Tibet, Climatic and Environ. Res., 6, 416–424, 2001.

Jia, S., Xu, X., Lin, W., Wang, Y., He, X., and Zhang, H.: Increased mixing ratio of surface ozone by nighttime convection process over the North China Plain, Journal of Applied Meteorological Science, 26, 280–290, 2015.

Kendall, M. G.: Rank Correlation Methods, Charles Griffin, London, 1955.

Lal, S., Venkataramani, S., Chandra, N., Cooper, O. R., Brioude, J., and Naja, M.: Transport effects on the vertical distribution of tropospheric ozone over western India, J. Geophys. Res.-Atmos., 119, 10012–10026, doi:10.1002/2014JD021854, 2014.

Langford, A. O., Aikin, K. C., Eubank, C. S., and Williams, E. J.: Stratospheric contribution to high surface ozone in Colorado during springtime, Geophys. Res. Lett., 36, L12801, doi:10.1029/2009GL038367, 2009.

Langford, A. O., Senff, C. J., Alvarez Ii, R. J., Brioude, J., Cooper, O. R., Holloway, J. S., Lin, M. Y., Marchbanks, R. D., Pierce, R. B., Sandberg, S. P., Weickmann, A. M., and

ACPD
15, 30987–31024, 2015

Williams, E. J.: An overview of the 2013 Las Vegas Ozone Study (LVOS): impact of stratospheric intrusions and long-range transport on surface air quality, Atmos. Environ., 109, 305–322, doi:10.1016/j.atmosenv.2014.08.040, 2015.

Lefohn, A. S., Wernli, H., Shadwick, D., Oltmans, S. J., and Shapiro, M.: Quantifying the importance of stratospheric–tropospheric transport on surface ozone concentrations at high- and low-elevation monitoring sites in the United States, Atmos. Environ., 62, 646–656, doi:10.1016/j.atmosenv.2012.09.004, 2012.

Lelieveld, J. and Dentener, F. J.: What controls tropospheric ozone?, J. Geophys. Res.-Atmos., 105, 3531–3551, doi:10.1029/1999JD901011, 2000.

Lin, M., Fiore, A. M., Cooper, O. R., Horowitz, L. W., Langford, A. O., Levy, H., Johnson, B. J., Naik, V., Oltmans, S. J., and Senff, C. J.: Springtime high surface ozone events over the western United States: quantifying the role of stratospheric intrusions, J. Geophys. Res.-Atmos., 117, D00V22, doi:10.1029/2012JD018151, 2012a.

Lin, M., Fiore, A. M., Horowitz, L. W., Cooper, O. R., Naik, V., Holloway, J., Johnson, B. J., Middlebrook, A. M., Oltmans, S. J., Pollack, I. B., Ryerson, T. B., Warner, J. X., Wiedinmyer, C., Wilson, J., and Wyman, B.: Transport of Asian ozone pollution into surface air over the western United States in spring, J. Geophys. Res.-Atmos., 117, D00V07, doi:10.1029/2011JD016961, 2012b.

Lin, M., Horowitz, L. W., Oltmans, S. J., Fiore, A. M., and Fan, S.: Tropospheric ozone trends at Mauna Loa observatory tied to decadal climate variability, Nat. Geosci., 7, 136–143, doi:10.1038/ngeo2066, 2014.

Lin, M., Fiore, A. M., Horowitz, L. W., Langford, A. O., Oltmans, S. J., Tarasick, D., and Rieder, H. E.: Climate variability modulates western US ozone air quality in spring via deep stratospheric intrusions, Nat. Commun., 6, 7105, doi:10.1038/ncomms8105, 2015a.

Lin, M., Horowitz, L. W., Cooper, O. R., Tarasick, D., Conley, S., Iraci, L. T., Johnson, B., Leblanc, T., Petropavlovskikh, I., and Yates, E. L.: Revisiting the evidence of increasing springtime ozone mixing ratios in the free troposphere over western North America, Geophys. Res. Lett., doi:10.1002/2015GL065311, online first, 2015b.

Lundquist, J. K.: Intermittent and Elliptical Inertial Oscillations in the Atmospheric Boundary Layer, J. Atmos. Sci., 60, 2661–2673, doi:10.1175/1520-0469(2003)060<2661:IAEIOI>2.0.CO;2, 2003.

ACPD
15, 30987–31024, 2015

Ma, J., Liu, H., and Hauglustaine, D.: Summertime tropospheric ozone over China simulated with a regional chemical transport model 1. Model description and evaluation, J. Geophys. Res.-Atmos., 107, 4660, doi:10.1029/2001JD001354, 2002a.

Ma, J., Tang, J., Zhou, X., and Zhang, X.: Estimates of the chemical budget for ozone at Waliguan observatory, J. Atmos. Chem., 41, 21–48, doi:10.1023/A:1013892308983, 2002b.

Ma, J., Zheng, X., and Xu, X.: Comment on "Why does surface ozone peak in summertime at Waliguan?" by Bin Zhu et al., Geophys. Res. Lett., 32, L01805, doi:10.1029/2004GL021683, 2005.

Ma, J., Lin, W. L., Zheng, X. D., Xu, X. B., Li, Z., and Yang, L. L: Influence of air mass downward transport on the variability of surface ozone at Xianggelila Regional Atmosphere Background Station, southwest China, Atmos. Chem. Phys., 14, 5311–5325, doi:10.5194/acp-14-5311-2014, 2014.

Monks, P. S.: A review of the observations and origins of the spring ozone maximum, Atmos. Environ., 34, 3545–3561, doi:10.1016/S1352-2310(00)00129-1, 2000.

Oltmans, S. J., Lefohn, A. S., Shadwick, D., Harris, J. M., Scheel, H. E., Galbally, I., Tarasick, D. W., Johnson, B. J., Brunke, E. G., Claude, H., Zeng, G., Nichol, S., Schmidlin, F., Davies, J., Cuevas, E., Redondas, A., Naoe, H., Nakano, T., and Kawasato, T.: Recent tropospheric ozone changes – a pattern dominated by slow or no growth, Atmos. Environ., 67, 331–351, doi:10.1016/j.atmosenv.2012.10.057, 2013.

Rao, A. R. and Hsu, E.-C.: Hilbert–Huang Transform Analysis of Hydrological and Environmental Time Series, 1st Edn., Water Science and Technology Library, 60, Springer Netherlands, 2008.

Sen, P. K.: Estimates of the regression coefficient based on Kendall's tau, J. Am. Stat. Assoc., 63, 1379–1389, 1968.

Staehelin, J., Harris, N. R. P., Appenzeller, C., and Eberhard, J.: Ozone trends: a review, Rev. Geophys., 39, 231–290, doi:10.1029/1999RG000059, 2001.

Stohl, A., Spichtinger-Rakowsky, N., Bonasoni, P., Feldmann, H., Memmesheimer, M., Scheel, H. E., Trickl, T., Hübener, S., Ringer, W., and Mandl, M.: The influence of stratospheric intrusions on alpine ozone concentrations, Atmos. Environ., 34, 1323–1354, doi:10.1016/S1352-2310(99)00320-9, 2000.

Tang, Q., Prather, M. J., and Hsu, J.: Stratosphere–troposphere exchange ozone flux related to deep convection, Geophys. Res. Lett., 38, L03806, doi:10.1029/2010gl046039, 2011.

ACPD
15, 30987–31024, 2015

Tarasova, O. A., Senik, I. A., Sosonkin, M. G., Cui, J., Staehelin, J., and Prévôt, A. S. H.: Surface ozone at the Caucasian site Kislovodsk High Mountain Station and the Swiss Alpine site Jungfraujoch: data analysis and trends (1990–2006), Atmos. Chem. Phys., 9, 4157–4175, doi:10.5194/acp-9-4157-2009, 2009.

Vingarzan, R.: A review of surface ozone background levels and trends, Atmos. Environ., 38, 3431–3442, doi:10.1016/j.atmosenv.2004.03.030, 2004.

Voulgarakis, A., Hadjinicolaou, P., and Pyle, J. A.: Increases in global tropospheric ozone following an El Niño event: examining stratospheric ozone variability as a potential driver, Atmos. Sci. Lett., 12, 228–232, doi:10.1002/asl.318, 2011.

Wang, Q. Y., Gao, R. S., Cao, J. J., Schwarz, J. P., Fahey, D. W., Shen, Z. X., Hu, T. F., Wang, P., Xu, X. B., and Huang, R. J.: Observations of high level of ozone at Qinghai Lake basin in the northeastern Qinghai-Tibetan Plateau, western China, J. Atmos. Chem., 72, 19–26, doi:10.1007/s10874-015-9301-9, 2015.

Wang, T., Ding, A., Gao, J., and Wu, W. S.: Strong ozone production in urban plumes from Beijing, China, Geophys. Res. Lett., 33, L21806, doi:10.1029/2006gl027689, 2006a.

Wang, T., Wong, H. L. A., Tang, J., Ding, A., Wu, W. S., and Zhang, X. C.: On the origin of surface ozone and reactive nitrogen observed at a remote mountain site in the northeastern Qinghai-Tibetan Plateau, western China, J. Geophys. Res.-Atmos., 111, D08303, doi:10.1029/2005JD006527, 2006b.

Wang, T., Wei, X. L., Ding, A. J., Poon, C. N., Lam, K. S., Li, Y. S., Chan, L. Y., and Anson, M.: Increasing surface ozone concentrations in the background atmosphere of Southern China, 1994–2007, Atmos. Chem. Phys., 9, 6217–6227, doi:10.5194/acp-9-6217-2009, 2009.

Wang, Y., Konopka, P., Liu, Y., Chen, H., Müller, R., Plöger, F., Riese, M., Cai, Z., and Lü, D.: Tropospheric ozone trend over Beijing from 2002–2010: ozonesonde measurements and modeling analysis, Atmos. Chem. Phys., 12, 8389–8399, doi:10.5194/acp-12-8389-2012, 2012.

Xu, W. Y., Lin, W. L., Xu, X. B., Tang, J., Huang, J. Q., Wu, H., and Zhang, X. C.: Long-term trends of surface ozone and its influencing factors at the Mt. Waliguan GAW station, China – Part 2: Variation mechanism and influencing factors, Atmos. Chem. Phys. Discuss., in preparation, 2015.

Xu, X., Lin, W., Wang, T., Yan, P., Tang, J., Meng, Z., and Wang, Y.: Long-term trend of surface ozone at a regional background station in eastern China 1991–2006: enhanced variability, Atmos. Chem. Phys., 8, 2595–2607, doi:10.5194/acp-8-2595-2008, 2008.

ACPD
15, 30987–31024, 2015

Xue, L. K., Wang, T., Zhang, J. M., Zhang, X. C., Deliger, Poon, C. N., Ding, A. J., Zhou, X. H., Wu, W. S., Tang, J., Zhang, Q. Z., and Wang, W. X.: Source of surface ozone and reactive nitrogen speciation at Mount Waliguan in western China: new insights from the 2006 summer study, J. Geophys. Res., 116, D07306, doi:10.1029/2010jd014735, 2011.

Yang, Y., Liao, H., and Li, J.: Impacts of the East Asian summer monsoon on interannual variations of summertime surface-layer ozone concentrations over China, Atmos. Chem. Phys., 14, 6867–6879, doi:10.5194/acp-14-6867-2014, 2014.

Zellweger, C., Hofer, P., and Buchmann, B.: System and performance audit of surface ozone and carbon monoxide at the China GAW baseline observatory Waliguan mountain, WCC-Empa Report 00/3Rep., Empa, Dübendorf, Switzerland, 46 pp., 2000.

Zellweger, C., Klausen, J., and Buchmann, B.: System and performance audit of surface ozone carbon monoxide and methane at the global GAW station Mt. Waliguan, China, October 2004, WCC-Empa Report 04/3Rep., Empa, Dübendorf, Switzerland, 52 pp., 2004.

Zellweger, C., Klausen, J., Buchmann, B., and Scheel, H.-E.: System and performance audit of surface ozone, carbon monoxide, methane and nitrous oxide at the GAW global station Mt. Waliguan and the Chinese academy of meteorological sciences (CAMS) China, June 2009, WCC-Empa Report 09/2Rep., Empa, Dübendorf, Switzerland, 61 pp., 2009.

Zhang, F., Zhou, L. X., Novelli, P. C., Worthy, D. E. J., Zellweger, C., Klausen, J., Ernst, M., Steinbacher, M., Cai, Y. X., Xu, L., Fang, S. X., and Yao, B.: Evaluation of in situ measurements of atmospheric carbon monoxide at Mount Waliguan, China, Atmos. Chem. Phys., 11, 5195–5206, doi:10.5194/acp-11-5195-2011, 2011.

Zhang, J. M., Wang, T., Ding, A. J., Zhou, X. H., Xue, L. K., Poon, C. N., Wu, W. S., Gao, J., Zuo, H. C., Chen, J. M., Zhang, X. C., and Fan, S. J.: Continuous measurement of peroxyacetyl nitrate (PAN) in suburban and remote areas of western China, Atmos. Environ., 43, 228–237, doi:10.1016/j.atmosenv.2008.09.070, 2009.

Zheng, X. D., Shen, C. D., Wan, G. J., Liu, K. X., Tang, J., and Xu, X. B.: ∼ (10)Be/∼ 7Be implies the contribution of stratosphere–troposphere transport to the winter-spring surface O_3 variation observed on the Tibetan Plateau, Chin. Sci. Bull., 56, 84–88, 2011.

Zhu, B., Akimoto, H., Wang, Z., Sudo, K., Tang, J., and Uno, I.: Why does surface ozone peak in summertime at Waliguan?, Geophys. Res. Lett., 31, L17104, doi:10.1029/2004GL020609, 2004.

Zou, H., Ji, C. P., Zhou, L. B., Wang, W., and Jiang, Y. X.: ENSO signal in total ozone over Tibet, Climatic and Environ. Res. 6, 267–272, 2001.

ACPD
15, 30987–31024, 2015

Table 1. The linear slope, 95 % confidence interval (in ppbv $10\,a^{-1}$) and the p values (in parenthesis) of seasonal average surface ozone concentration during 1994 to 2013.

Data subset	MAM	JJA	SON	DJF
All Day	2.4 ± 1.1 (< 0.01)	1.5 ± 1.9 (0.12)	2.8 ± 1.1 (< 0.01)	1.4 ± 0.9 (< 0.01)
Day	2.4 ± 1.1 (< 0.01)	0.7 ± 1.8 (0.41)	2.7 ± 1.0 (< 0.01)	1.5 ± 0.9 (< 0.01)
Night	2.4 ± 1.2 (< 0.01)	2.2 ± 2.0 (0.04)	2.9 ± 1.1 (< 0.01)	1.3 ± 1.0 (0.01)

ACPD
15, 30987–31024, 2015

Table 2. The linear slope (in ppbv $10\,a^{-1}$) and the 95 % confidence interval of all-year and seasonal average surface ozone concentration during 1994 to 2013 at north hemispheric high altitude GAW sites.

Station (Location)	Time Span	All Year	MAM	JJA	SON	DJF	Reference
Mauna Loa, USA (19.5° N, 155.6° W, 3397 m a.s.l.)	1991–2010	3.1 ± 0.7					Oltmans et al. (2013)
Izaña, Spain (28.3° N, 16.5° W, 2367 m a.s.l.)	1991–2010	1.4 ± 0.5					Oltmans et al. (2013)
Waliguan, China (36.3° N, 100.9° E, 3816 m a.s.l.)	1994–2013	2.5 ± 1.7	2.4 ± 1.1	1.5 ± 1.9	2.8 ± 1.1	1.4 ± 0.9	This work
Rocky, USA (40.3° N, 105.6° W, 2743 m a.s.l.)	1991–2010	3.3 ± 0.5					Oltmans et al. (2013)
Pinadale, USA (42.9° N, 109.8° W, 2743 m a.s.l.)	1991–2010	−0.5 ± 0.4					Oltmans et al. (2013)
Kislovodsk, Russia (43.70° N, 42.70° E, 2070 m a.s.l.)	1991–2006	−3.7 ± 1.4	−2.0 ± 2.0	−1.4 ± 2.4	−6.0 ± 2.1	−3.0 ± 2.5	Tarasova et al. (2009)
Whiteface, USA (44.4° N, 73.9° W, 1484 m a.s.l.)	1991–2010	−2.2 ± 0.6					Oltmans et al. (2013)
Jungfraujoch, Switzerland (46.5° N, 8.0° E, 3580 m a.s.l.)	1990–2008	3.2 ± 1.8	3.3 ± 2.2	2.2 ± 2.8	3.3 ± 1.6	4.9 ± 1.7	Cui et al. (2011)
Zugspitze, Germany (47.4° N, 11.0° E, 2960 m a.s.l.)	1991–2010	0.5 ± 0.4					Oltmans et al. (2013)

ACPD
15, 30987–31024, 2015

Table 3. Modified Mann–Kendall trend test on segments based on the last IMF.

Segment	Time Range	Slope of c5	Modified Mann–Kendall test (z)	Slope of O_3 (ppbv $10\,a^{-1}$)
1	Aug 1994–Jun 1997	–	No significant trend (z = 1.42)	2.7
2	Jul 1997–May 2002	+	Significant upward trend (z = 3.66)	4.2
3	Jun 2002–Apr 2008	–	Significant upward trend (z = 3.57)	3.0
4	May 2008–Jul 2013	+	Significant upward trend (z = 3.42)	3.6

ACPD
15, 30987–31024, 2015

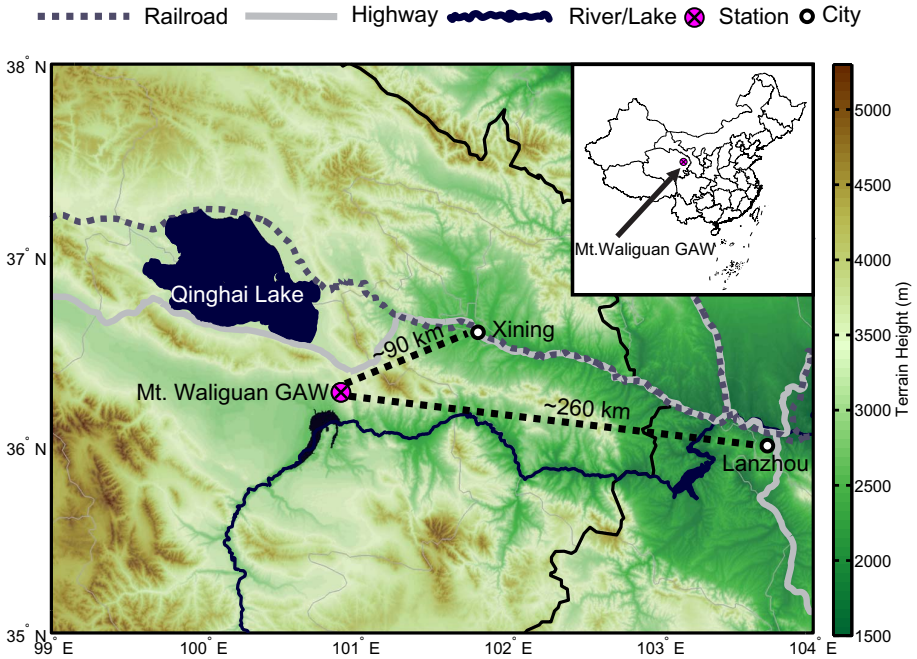

Figure 1. The location of the Mt. Waliguan GAW site and the two major cities in its vicinity. The shading stands for the topographic height.

ACPD
15, 30987–31024, 2015

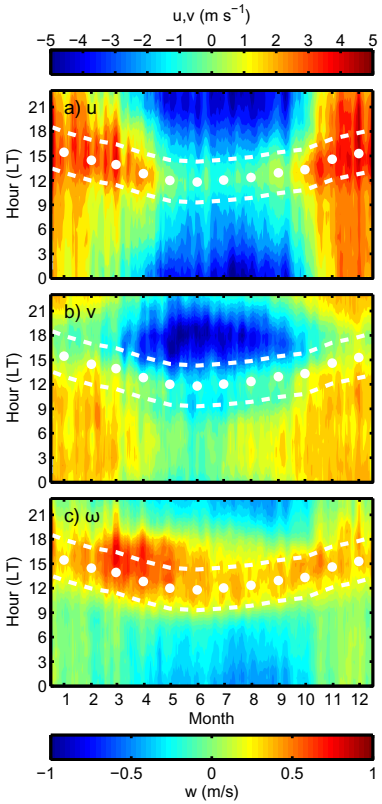

Figure 2. The average season-diurnal variation of surface zonal **(a)**, meridional **(b)** and vertical **(c)** wind veclocity on top of Mt. Waliguan during 1995–2013. The monthly average hour associated with the diurnal maximum zonal wind speed is given by the white dots, the daytime range is provided by the white dashed lines, which covers 6 h centered around the white dots.

ACPD
15, 30987–31024, 2015

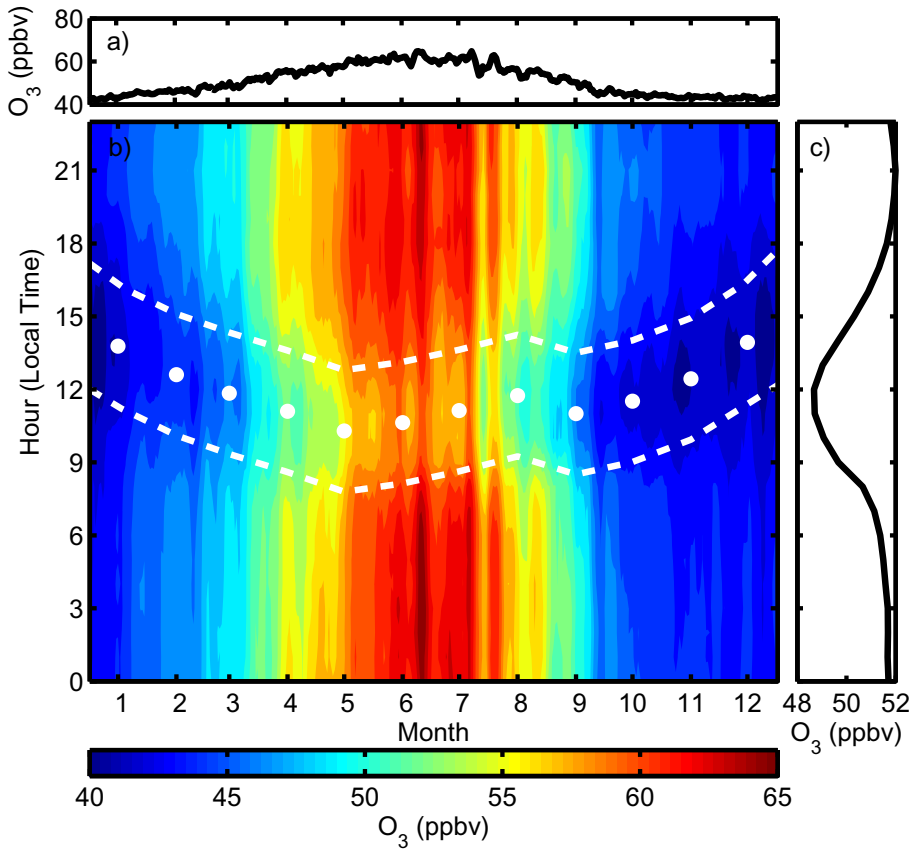

Figure 3. The average seasonal variation **(a)**, season-diurnal variation **(b)** and diurnal variation **(c)** of ozone during 1995 to 2013. White dots stands for the monthly average local time associated with the diurnal minimum ozone, the white dashed line stands for a 6 h range centered around the white dots.

ACPD
15, 30987–31024, 2015

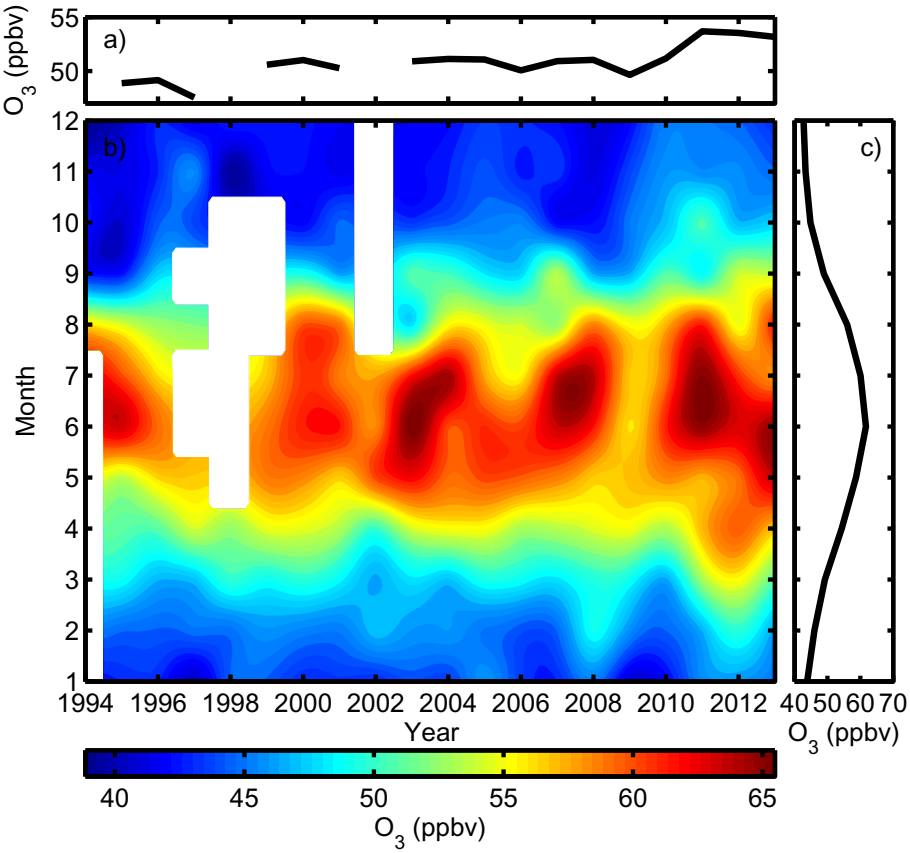

Figure 4. The average inter-annual variation **(a)**, season-annual variation **(b)** and seasonal variation **(c)** of ozone during 1994 to 2013.

ACPD
15, 30987–31024, 2015

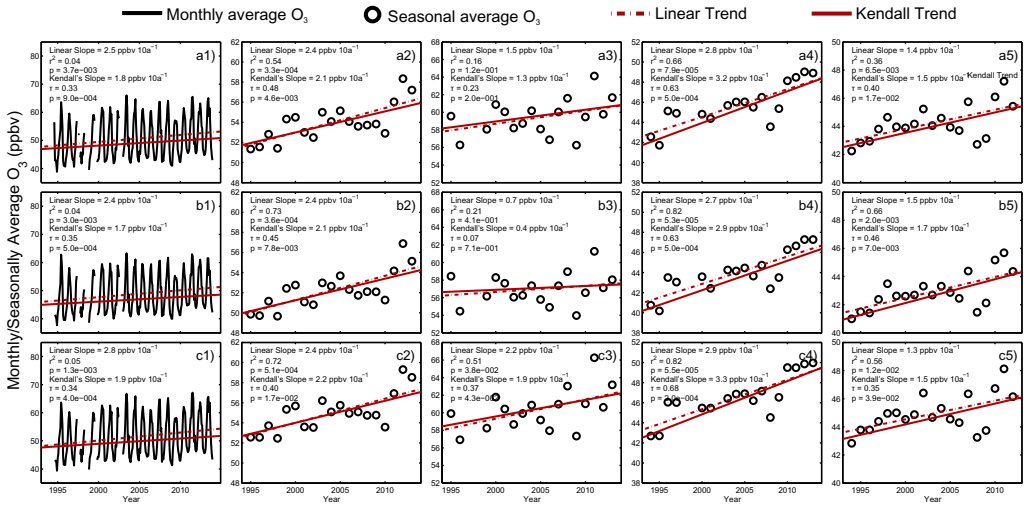

Figure 5. (1) Monthly, (2) spring (MAM), (3) summer (JJA), (4) autumn (SON) and (5) wintier time average all day **(a)**, daytime **(b)** and nighttime **(c)** surface ozone concentration during 1994 to 2013 (black solid line or black circles) and its variation trend (red lines: dotted line stands for the linear variation and solid line stands for the Kendall's variation slope).

ACPD
15, 30987–31024, 2015

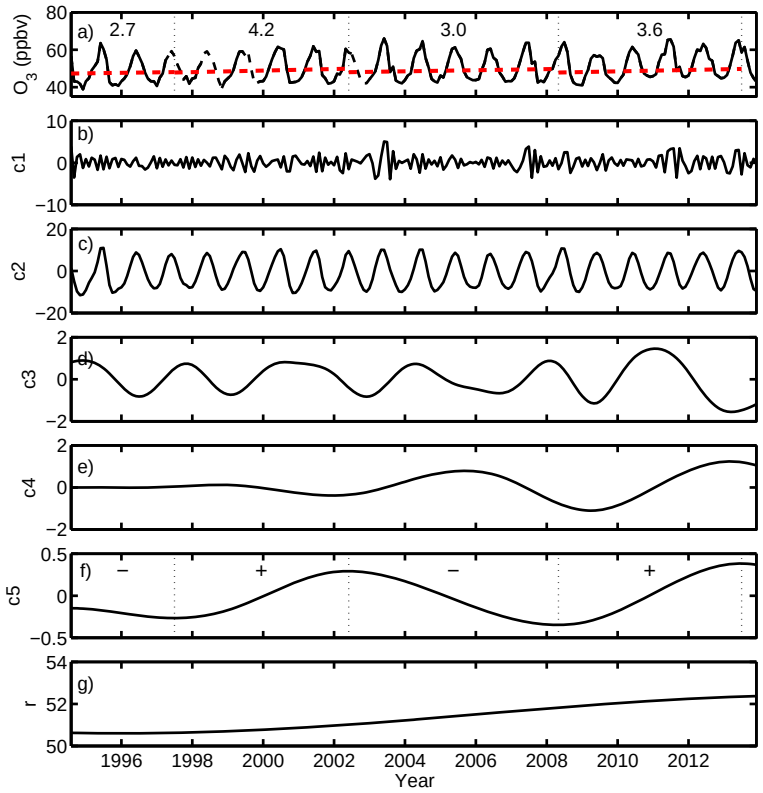

Figure 6. The interpolated monthly average ozone concentration at WLG from 1994 to 2013 (the interpolated data given in dashed lines, **(a)** and its intrinsic mode functions (c1–c5) **(b–f)** and its residue, *r* **(g)**. The time segments in **(a)** were determined by the slope of the (c5). The red slashed lines are the Kendall's trends and the numbers are the Kendall's slope (in ppbv a^{-1}).

ACPD
15, 30987–31024, 2015

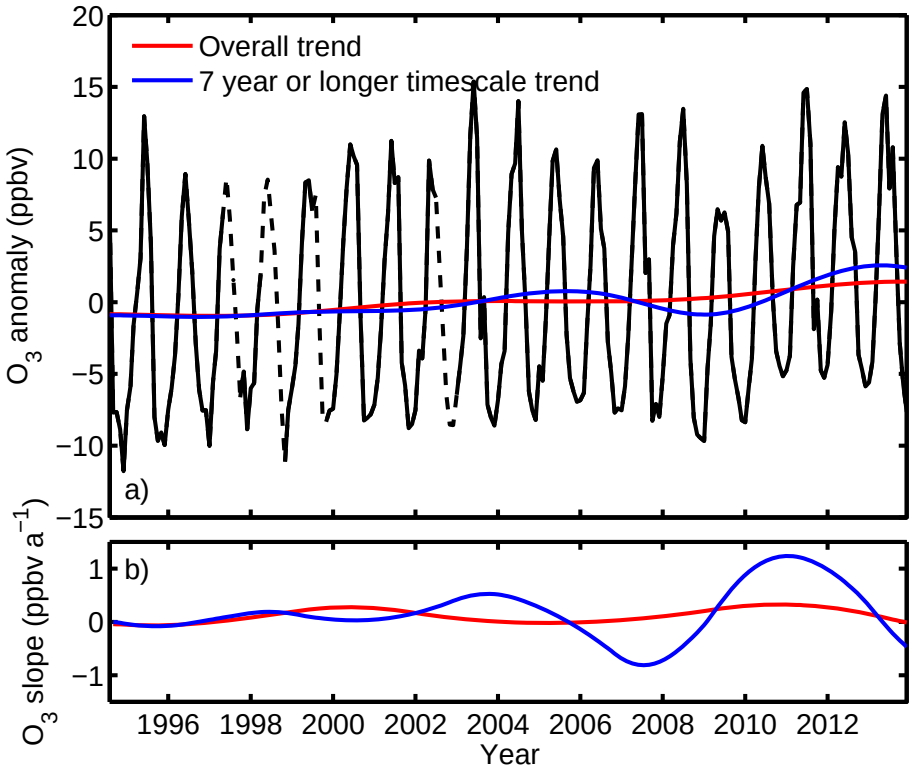

Figure 7. (a) The anomaly of the interpolated monthly average ozone (black line) the sum of last IMF and the residual (c5 + *r*, red line) and the sum of the last two IMFs and the residual (c4 + c5 + *r*, blue line); **(b)** the slope of the sum of last IMF and the residual (c5 + *r*, red line) and the sum of the last two IMFs and the residual (c4 + c5 + *r*, blue line).

ACPD
15, 30987–31024, 2015

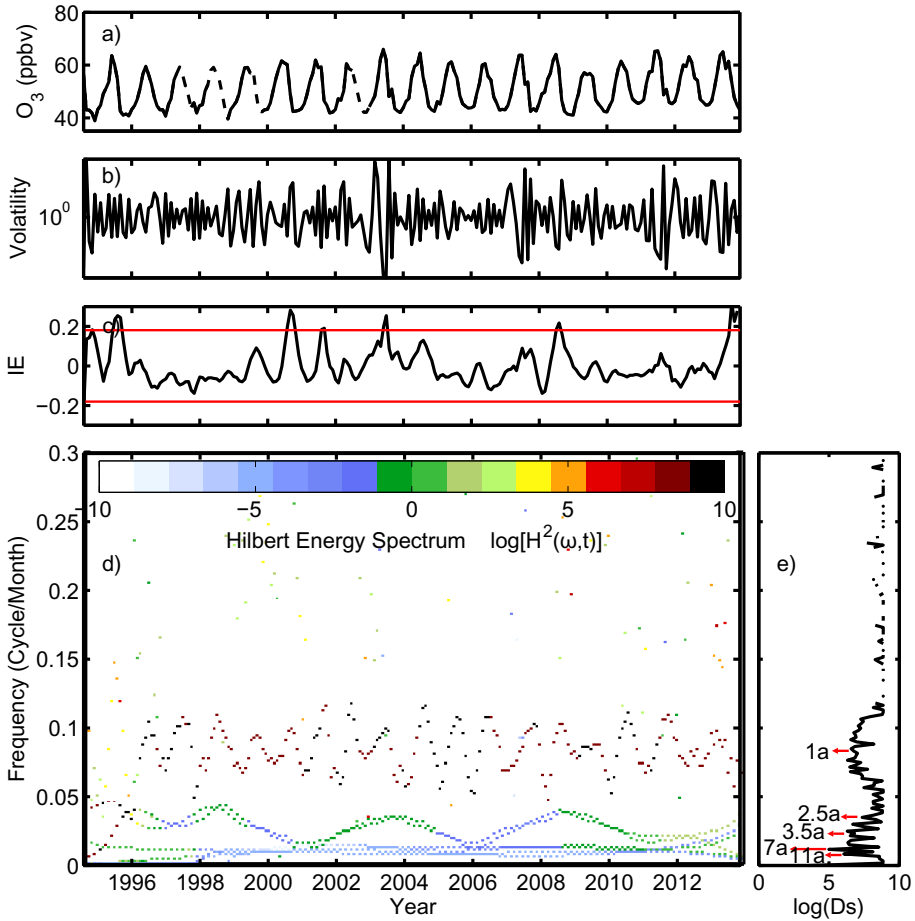

Figure 8. The interpolated monthly average ozone concentration signal at Mt. WLG during 1994 to 2013 **(a)**, the volatility **(b)**, the normalized mean value of the instantaneous energy (red lines: $\pm 2\sigma$) **(c)**, Hilbert Energy Spectrum **(d)** and the degree of stationarity **(e)**.

ACPD
15, 30987–31024, 2015